JOURNAL OF SPACECRAFT AND ROCKETS
Vol. 43, No. 1, January–February 2006

Mach 6 Boundary-Layer Stability Experiments on Sharp and Blunted Cones

Anatoly A. Maslov,* Alexander N. Shiplyuk,† Dmitry A. Bountin,‡ and Andrey A. Sidorenko§
Russian Academy of Sciences, 630090, Novosibirsk, Russia

Recent studies of hypersonic boundary-layer stability and transition on cones with sharp and blunted nosetips are presented. The experiments were carried out on a 7-deg half-angle cone at freestream Mach number 5.95. Laminar–turbulent transition locations are measured for various flow parameters and model nose bluntness. Mean and fluctuation characteristics of the flow are obtained using constant-temperature hot-wire anemometry. The spectral content and amplification rates of natural disturbances are obtained. The method of artificial wave packets is applied to obtain detailed information on the disturbances. Data on development of both natural and artificial finite-amplitude disturbances are compared. It is experimentally shown that the wave vector of the most unstable waves of the first mode have an inclination angle of 40–49 deg. In the frequency range of the second mode, plane waves appear to be dominant and have the highest amplification. The bluntness of the cone nosetip results in an increase of the disturbance amplification rate downstream of the entropy layer swallowing point. At the same time, nose bluntness dramatically increases the transition Reynolds number because of the strong damping of initial disturbances.

Nomenclature

A = amplitude of pulsations, arbitrary units
$|A_f|$ = amplitude of a wave at frequency f, arbitrary units
C_x = longitudinal phase velocity of disturbances, m s^{-1}
F = dimensionless frequency $F = 2\pi f/(Re_{1e}U_e)$
f = frequency, Hz
M = Mach number
N = number of samples in Fourier decomposition
P = pressure, Pa
R = $\sqrt{(Re_{1e} \cdot x)}$ (Reynolds number based on distance form nosetip to hot-wire probe)
Re = Reynolds number
Re_1 = unit Reynolds number, m^{-1}
T = temperature, K
t = time, s
U = flow velocity, m s^{-1}
V = anemometer output voltage, V
$V(x, y, \theta, t_j)$ = oscillogram of alternate hot-wire signal
x, y, z = Cartesian coordinates, mm
α_i = amplification rate
α_r = longitudinal wave number, rad mm^{-1}
β = transversal (azimuthal) wave number, rad deg^{-1}
δ = boundary-layer thickness, mm
θ = model rotation angle, deg
λ = wave length, mm
ρ = density, kg m^{-3}
Φ = phase of pulsations, rad
χ = incidence angle of wave vector in the xz plane, deg
$\langle\,\rangle$ = rms value of parameter

Subscripts

e = parameter on the boundary layer edge
w = parameter on the model wall
0 = stagnation parameter
∞ = freestream parameter

Superscript

$\bar{}$ = mean value

Introduction

ONE of the key problems with development of hypersonic aircraft is the prediction and control of boundary-layer transition. Unlike the case of sub- and supersonic flow velocities, the mechanisms underlying the laminar–turbulent transition in hypersonic flows still remain poorly understood, because of difficulties in performing experimental and theoretical studies of such flows, and because of the intricate nature of the physical processes giving rise to turbulence. At hypersonic velocities, for Mach numbers greater than $M \approx 4$–4.5, in addition to the vortex instability mode, there arises a new, acoustic type of instability (the so-called second mode). According to numerical studies,[1] the second mode in hypersonic flows is the most unstable instability and is expected to govern the occurrence of the laminar–turbulent transition. These findings are confirmed by wind-tunnel experiments. However, in a number of experiments[2,3] the second mode is shown not to prevail in hypersonic boundary layers.

For hypersonic flows, the influence of the mean-flow features of hypersonic boundary layers on the development of vortex and acoustic modes and on the location of the transition point also remains poorly understood. In particular, of practical importance are studies of the stabilizing action of the leading-edge bluntness and the nonunique effect of bluntness radius on the degree of stabilization. There are just a few experimental studies of the effect of bluntness on the stability of the hypersonic boundary layer.[4,5]

Gaining data on characteristics of initial boundary-layer perturbations is another problem with stability studies at hypersonic velocities. These initial characteristics largely affect the downstream

---

Received 1 February 2004; accepted for publication 10 September 2004.

*Professor and Deputy Director, Institute of Theoretical and Applied Mechanics, Siberian Branch; maslov@itam.nsc.ru. Member AIAA.

†Senior Researcher, Hypersonic Flow Laboratory, Institute of Theoretical and Applied Mechanics, Siberian Branch; shiplyuk@itam.nsc.ru.

‡Junior Researcher, Hypersonic Flow Laboratory, Institute of Theoretical and Applied Mechanics, Siberian Branch; bountin@itam.nsc.ru.

§Senior Researcher, Hypersonic Flow Laboratory, Institute of Theoretical and Applied Mechanics, Siberian Branch; sindr@itam.nsc.ru.

evolution of the spectra and amplification rates of disturbances. The initial disturbances are usually generated near the leading edge of the model. In this zone, the Reynolds numbers are still low, and the boundary-layer flow represents a viscous shock layer. The present paper describes experimental results that clarify in part some of these questions.

Instrumentation and Measurement Procedure

The experiments were carried out in the T-326 hypersonic wind tunnel of the Institute of Theoretical and Applied Mechanics, Siberian Branch, Russian Academy of Sciences. This facility is a blowdown wind tunnel of the ejector type that exhausts to atmosphere. The duration of the continuous tunnel run is determined by the configuration of the contoured nozzle, and for Mach number 5.95 the run time is 30 min. The model is placed in the open-jet test section, which has a core flow diameter of 180 mm. To avoid condensation, the air is heated with an electrical heater. The wind tunnel is equipped with a three-component traversing mechanism to move the hot-wire probe along the x, y, and z coordinates. The position of the probe is controlled with an accuracy of 0.01 mm. Its zero (reference) position at the model surface is identified by an electrical contact between the probe and the model surface. The model support provides rotation of the model around its axis with an accuracy of 0.1 deg. To move the pitot probe in the boundary layer, a second traversing gear with an accuracy of 0.1 mm is used.

In the stability experiments the stagnation pressure is $P_0 = 9.8 \times 10^5 \pm 0.1\%$ Pa and the stagnation temperature is $T_0 = 380 \pm 0.9\%$ K, which correspond to a unit Reynolds number $Re_{1\infty} = 12.2 \times 10^6$ m^{-1}. The freestream Mach number M_∞ is $5.95 \pm 0.8\%$. In the transition location experiments the stagnation pressure is varied in the range from 9.8 to 19.5 Pa corresponding to unit Reynolds number $(12.2\text{–}22.6) \times 10^6$ m^{-1}. All experiments are carried out under adiabatic wall model conditions.

The model (Fig. 1) is a 0.5-m-long steel cone with a 7-deg half-angle. The cone is exposed to the flow at zero angle of attack by means of surface pressure measurements at two pairs of diametrically opposite locations. Accuracy of this method is defined by the pressure measurement accuracy, which is 1.2% of measured pressure (1250 Pa). The smallest pressure difference that can be resolved by two sensors is 2.4%. The pressure difference between two diametrically opposite points is about 2.5%, when the cone is under a 0.1-deg angle of attack, which gives the cone an alignment accuracy of 0.1 deg. The model is assembled with one of three interchangeable noses: a sharp nose with a bluntness radius smaller than 0.1 mm, and two blunted noses with bluntness radii of 2 and 20 mm. Because of its relatively large mass, the cone takes a long time to heat up to adiabatic temperature in the hypersonic flow. Therefore the model is equipped with an internal heater, which, before each wind-tunnel run, heats the model close to the recovery temperature ($T_w \approx 320$ K). At the beginning of each run the model is additionally heated by the flow, and therefore a temperature distribution corresponding to adiabatic conditions is more quickly attained. The wall temperature is measured by a thermocouple that is embedded into the model and located near its surface.

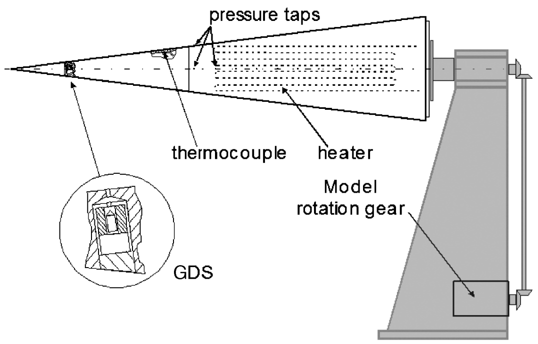

Fig. 1 Model of a 7-deg half-angle cone equipped with GDS.

To excite artificial disturbances in the boundary layer the model is equipped with a glow discharge source (GDS). The operation of this device is based on a high-frequency electric glow discharge in a chamber beneath the model surface. Periodic pulsations penetrate into the boundary layer through an orifice of diameter 0.4 mm. A similar GDS design was used for excitation of artificial disturbances in the hypersonic boundary layer by Arnal et al.[6] This kind of disturbance source has some obvious advantages, such as high frequency, stable phase, and absence of mean flow distortion. In the design chosen for the present experiment, the sharp central electrode is the cathode and the model body is used as the anode. The GDS is driven by high-voltage unidirectional periodical pulses with amplitudes up to 700 V.

The position of the laminar–turbulent transition is determined using a pitot probe of circular section 0.7 mm in diameter. The pitot probe is traversed in the boundary layer along the cone generatrix, at a constant distance from the wall. The transition point is identified as a maximum in the pitot pressure distributions, which corresponds to the end of the transition.[7] The pitot pressure is measured with an accuracy of 0.5% by a strain-gauge transducer having a range of 0–10^5 Pa.

The flow parameters in the boundary layer are measured with a custom-made constant-temperature hot-wire anemometer that has a bandwidth up to 500 kHz. Single-wire probes made from a tungsten wire 5 μm in diameter and 1.3 mm long are used. The overheat ratio of the probe wire is 0.4. It is assumed in the data processing that the anemometer is mainly sensitive to mass-flow pulsations, because the mass-flow fluctuations are much larger than the temperature fluctuations.[6]

The output signal of the hot wire is split into dc and ac components and both components are digitized separately by means of two 12-bit analog-to-digital converters (ADCs) with a sampling rate of 1.25 MHz. At each location of measurement both ADCs are started at the same instant and 32,000 samples each are recorded. For the ac component the data are acquired in different ways for the experiments with natural and artificial disturbances. In the case of natural disturbances the ADC is triggered once and one continuous record is acquired. In the artificial disturbance experiments the whole record is split into 100 records of 1024 samples per record and then averaged. The triggering is set so that the start of each record is synchronized with the source voltage to the ADC.

Vertical profiles of voltage and mass flow fluctuations in the boundary layer are measured. To obtain mass flow fluctuation from hot-wire measurement data it is assumed[6] that

$$\rho U / \overline{\rho U} = V / \bar{V} \cdot K_{\mathrm{exp}}$$

where the coefficient K_{exp} is 0.25.

Measurements in the layer of maximum pulsations are made to obtain spatial amplification rates of disturbances. For these measurements the hot-wire probe is traversed along the model generatrix while positioned at the location of maximum pulsation in the vertical direction. At each point of measurement a spectral analysis of the hot-wire signal is performed.

The amplification rates α_i of disturbances are calculated as

$$-\alpha_i = \frac{1}{2|A_f|} \frac{\partial |A_f|}{\partial R}$$

The calculation procedure included the smoothing of the distributions of amplitude of longitudinal pulsations. The amplitude distributions are smoothed first by a running average method, and then by a Gaussian kernel method. After this the distributions are fitted by fourth-order polynomials.

In the study, the method of artificial wave packets is used.[8] A periodic point electrical discharge is used as the source of disturbances. It generates a wave packet that travels and develops in the boundary layer. This wave packet can be represented as a set of plane harmonic waves with various angles of incidence for comparison with the hydrodynamic stability theory predictions. To isolate the plane waves from the wave packet the following technique is applied. The hot-wire probe is moved in the streamwise direction, while staying in the maximum pulsation layer, and the model is rotated to scan the region of wave packet development. At each location of measurement the probe is stopped and hot-wire signal records are acquired. Because the ADC is triggered together with the GDS, a Fourier decomposition of time series is applied to extract amplitude A and phase Φ of disturbances at each location of the hot wire:

$$A_f(x, y, \theta) \cdot e^{i\Phi(x,y,\theta)} = \frac{2}{N}\sum_{j=1}^{N} V(x, y, \theta, t_j) \cdot e^{-i\omega t_j}$$

To study the spatial structure of the wave packet, the spatial distributions of A and Φ are expanded into series in azimuthal wavenumbers by applying a discrete space Fourier transform:

$$A_{f\beta}(x, \beta) = \frac{2}{N}\sum_{j=1}^{N} A_f(x, \theta_j) e^{-i\beta\theta_j}$$

Because of the weak dependence of the disturbance phase velocity C_x on the inclination angle, the phase velocity is determined from phase measurements in the center of the wave packet.[1] In this case a longitudinal wave number α_r is estimated by the formula $\alpha_{r\beta=0} = \Delta\Phi/\Delta x$ and the disturbance phase velocity is given as $C_x = (\lambda \cdot f)/U_e$, where $\lambda = 2\pi/\alpha_r$ is the wavelength of a disturbance. The angle of wave vector inclination is calculated as $\chi = \mathrm{arctg}(\beta_z/\alpha_r)$, where β_z, the wave number along the z coordinate, depends on β and the local arc length.

The frequency range of the artificial disturbances introduced into the flow is chosen based on the measured data for the evolution of natural boundary-layer disturbances. From the frequency spectra of the natural pulsations, two frequencies are chosen, $f_1 = 78$ kHz and $f_2 = 269$ kHz, which correspond to the most unstable disturbances of the first and second modes.

Results and Discussion

Laminar–Turbulent Transition Location

Figure 2 shows the dependence of the transition Reynolds number Re_1, calculated from the parameters at the outer edge of the boundary layer, on the Mach number M_e (Ref. 9). Here data from flight experiments, calculations based on the e^N method for adiabatic and cold-wall conditions, and results of transition measurements in conventional and quiet wind tunnels are shown. In the same figure, data of the present study are also plotted. The transition Reynolds numbers obtained in the T-326 wind tunnel (which, as a matter of fact, cannot be considered as a quiet facility) lie well above the generalized curve of conventional wind tunnel data. The main reason is that data from Ref. 9 show the beginning of transition, whereas our data display the end of transition.

In the experiments with blunted cones, no laminar–turbulent transition is found; i.e., the boundary layer is found to remain laminar along the full model length under the conditions of the experiments. This is indicative of the strong stabilizing action of bluntness for the chosen values of bluntness radii.

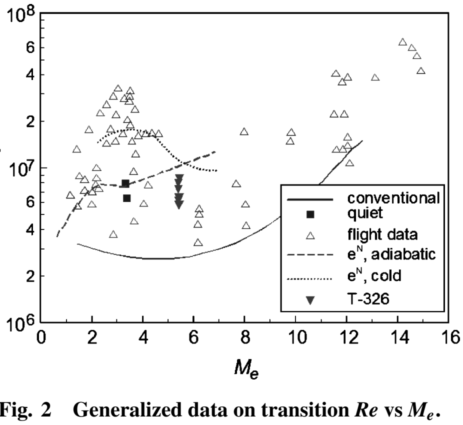

Fig. 2 Generalized data on transition Re vs M_e.

Development of Natural Disturbances

Mean flow and pulsation characteristics in the boundary and entropy layers are measured with a hot-wire anemometer. Figure 3 shows the distributions of the mean anemometer output signal (V) and the rms pulsation amplitudes of the mass flux ($\langle\rho U\rangle$) across the boundary and entropy layers for all the three bluntnesses. The anemometer output signal V is normalized to its value at the outer edge of the boundary layer V_e; the values of $\langle\rho U\rangle$ are expressed as percentages of the mean value of the local mass flux ρU; and the coordinate y is normalized to the boundary-layer thickness (δ). The coordinate x is along the cone generatrix and is measured from the tip of the model nose (for the blunted cones, x is measured from the actual blunted nosetip). Distributions measured on the sharp cone (Fig. 3a) have a shape that is typical of a hypersonic laminar boundary layer. In Fig. 3a, at the last measurement section, the widening of the disturbed region across the layer and the deformation of the mean flowfield, which are both related to the laminar–turbulent transition on the sharp cone, are shown.

Because the bow shock is curved ahead of a blunt cone, an entropy layer is formed. The region of the entropy layer may be noted by the dissimilarity of the mean-voltage profiles: at the first measurement

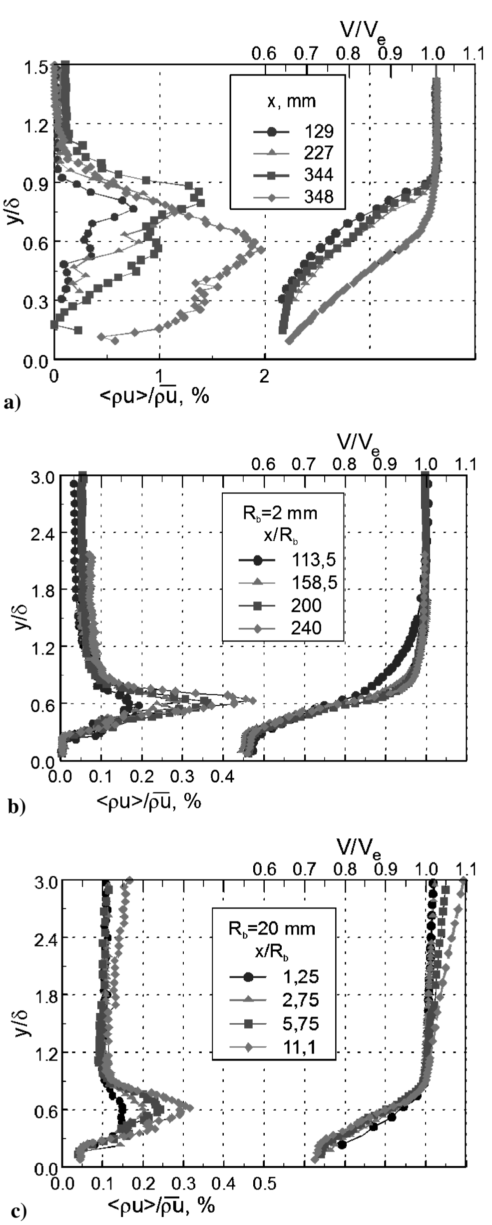

Fig. 3 Vertical distributions of the mean hot-wire signal and mass flow pulsations in the boundary layer for a) sharp model; b) blunted model, $R_b = 2$ mm; and c) blunted model, $R_b = 20$ mm.

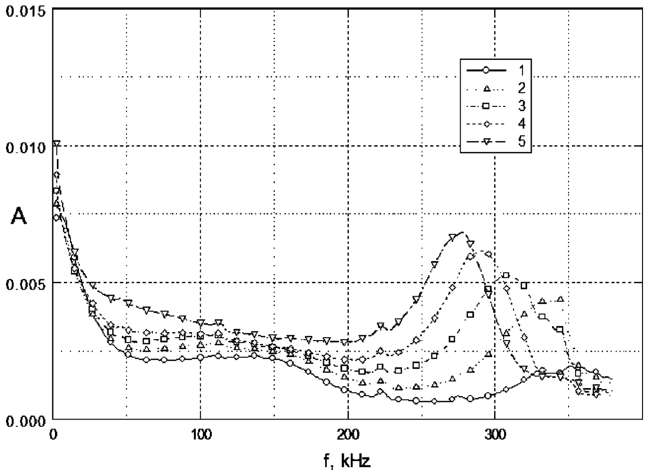

Fig. 4 Fourier spectra of the hot-wire data along the sharp cone: 1, $x = 193$; 2, $x = 218$; 3, $x = 243$; 4, $x = 268$; and 5, $x = 293$ mm.

station it results, for $y \approx \delta$, in differences from the remaining profiles in Fig. 3b ($R_b = 2$ mm), and the profiles in Fig. 3c are not similar for $y > \delta$. In Fig. 3b the mean-voltage profiles are similar after the first measurement station, indicating that the entropy layer has already been swallowed by the boundary layer. The coordinates of the point where the boundary layer fully absorbs the entropy layer are found to agree well with those predicted by Rotta's[10] method (measured, 415 mm; predicted, 407 mm). For large bluntness radii ($R_b = 20$ mm), the mean profiles exhibit changes throughout the whole measurement region because the entropy layer in this case does not vanish (Fig. 3c). The absorption coordinate predicted by Rotta's method is 8.8 m. The shape of the flow pulsation profiles in Figs. 3b and 3c remain unchanged, which shows that the boundary-layer flow-is laminar and the level of flow pulsations in the case of interest is substantially lower than that in the region of laminar flow on a sharp cone. Also, it is important to notice that the pulsation level in the entropy layer is very small and has the same order as the free stream pulsations.

Fourier spectra of the hot-wire data measured in the layer of the maximum pulsation along the sharp cone are shown in Fig. 4. It is clearly seen that the pulsations are grouped into two frequency ranges, $f = 50$–200 and 250–350 kHz. The peak of flow pulsations in the high-frequency region corresponds to the second mode and is always present in the spectra for the sharp cone; sometimes it is also observed in the spectra for the blunted cone with $R_b = 2$ mm and its amplitude is appreciably smaller. For the cone with $R_b = 20$ mm, it is never observed. With increasing R, the position of the peak on the frequency scale is moved toward lower frequencies; this moment is associated with the increase of δ and is typical for the second mode. Strong amplification of the second mode is also seen.

Figures 5a and 5b show the amplification rate $-\alpha_i$ vs the frequency f for the sharp cone and for the cone with $R_b = 2$ mm respectively. The local maxima at low frequencies ($f \approx 100$ kHz for the sharp cone and $f \approx 50$ kHz for the blunted one) correspond to the first-mode disturbances. The peaks at high frequencies ($f \approx 250$–300 kHz for the sharp cone and $f \approx 180$–200 kHz for the blunted cone) correspond to the second mode. As the R increases, the frequency of the second mode decreases, which is characteristic of this type of instability (Fig. 5a). It is easy to see that the growth rates of the second mode on the sharp cone are appreciably greater than the growth rates of the first mode. The amplification rates of low-frequency disturbances on the cone with the blunted nose increase slightly, whereas the amplification rates corresponding to the second mode increase rapidly to the values observed in the case of the sharp cone. The rapid increase of $-\alpha_i$ and, hence, of the pulsation amplitudes corresponding to the second mode is observed in the region downstream of the point where the boundary layer fully absorbs the entropy layer ($R \approx 2620$).

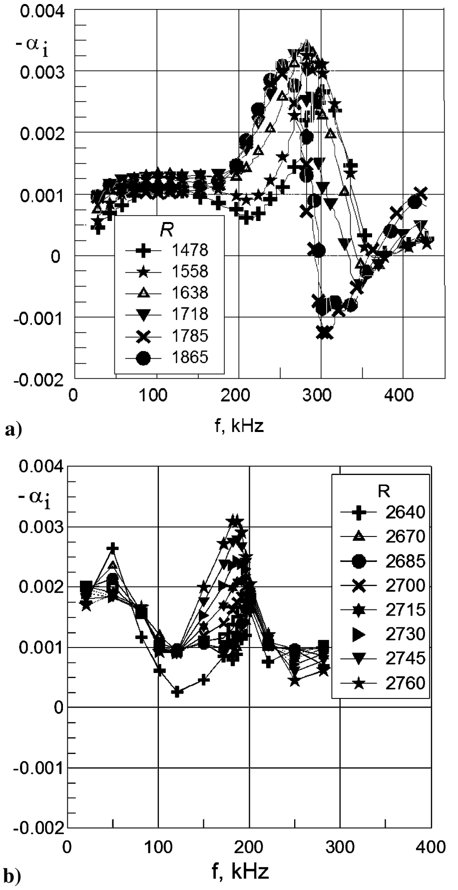

Fig. 5 Amplification rate $-\alpha_i$ vs frequency f for the a) sharp and b) blunted cone.

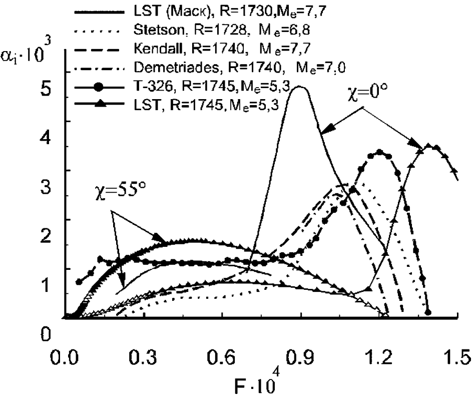

Fig. 6 Dependence of $-\alpha_i$ for a sharp cone on the frequency parameter F.

Figure 6 shows the dependence of $-\alpha_i$ on the frequency parameter F obtained theoretically by Mack, and experimentally by Stetson et al.[11] In the same graph, experimental data of the present study (sharp cone) and results of numerical studies based on a linear stability theory (LST)[12] are plotted. Stability calculations were based on the linear stability equations (Dann–Lin equations). Mean flow was obtained as a solution of the self-similar boundary layer equations.

The experimental data are seen to be in good qualitative and satisfactory quantitative agreement with each other. The discrepancy between the frequencies of the disturbances with the largest $-\alpha_i$ obtained in the different studies is likely caused by the difference in the Mach numbers explored. The substantial discrepancy between the experimental and predicted values may be explained by nonparallelism of the actual boundary-layer flows, which is not accounted for in simulations. The difference in values of $-\alpha_i$ is most likely caused by experimental error and the derivation procedure.

Evolution of Artificial Disturbances

To obtain the spatial structure of the boundary-layer perturbations, artificial wave packet development was investigated on the sharp cone. The measured phase and amplitude space distributions of the introduced disturbances are used as the basis for the calculations of the azimuthal wavenumbers.

Figure 7 shows the vertical distribution of pulsation amplitude for natural and artificial disturbances compared with LST calculation. The measured phase velocity $C_x = 0.89$ of artificial disturbances at 78 kHz ($F = 0.38 \times 10^{-4}$) is in excellent agreement with LST calculation ($C_x = 0.89$) for the first mode. The azimuthal wave number spectra (Fig. 8) are seen to exhibit two distinct symmetrical peaks in the region $\beta \approx \pm 0.3$ rad/deg. Depending on the position of the cross section ($x = 169$–229 mm), a pair of oblique waves with wave vectors is directed at angles $\chi = \pm 40$–49 deg correspond to these peaks. This agrees with theory, which predicts dominance of oblique waves for the first mode. Taking into account the phase speed and spatial-wave structure, it can be concluded that the excited disturbances are waves of the first mode.

Weak waves with strong inclination angle ($\chi \approx 70$ deg) are noticeable in all spectra. We suppose that these waves appear from nonlinear processes. Our present investigations (not yet published) show that the nonlinear effects in this region are weak and do not affect the evolution of the main waves ($\beta \approx \pm 0.3$ rad/deg). An estimate of the amplification rates of the most unstable ($\chi = 40$–49 deg) disturbances gives $-\alpha_i = (9\text{–}17) \times 10^{-4}$.

LST calculation of phase velocity of the second mode disturbances at 269 kHz ($F = 1.294 \times 10^{-4}$) gives a value of $C_x = 0.914$, which is close to the measured value ($C_x = 0.9$). The azimuthal wavenumbers spectra of the artificial wave packets are shown in Fig. 9. These spectra display a narrow peak at $\beta = 0$. At the first position there are two closely spaced components (oblique waves with small inclinations angles), but downstream only one component, corresponding to a wave with an inclination angle of $\chi = 0$ deg, is present. Figure 9 therefore shows the prevalence of a two-dimensional wave in the packet. Thus, the most rapidly growing disturbances at the frequency of interest are two-dimensional perturbations. The latter confirms theoretical predictions and agrees with the experimental data of Poggie and Kimmel.[13]

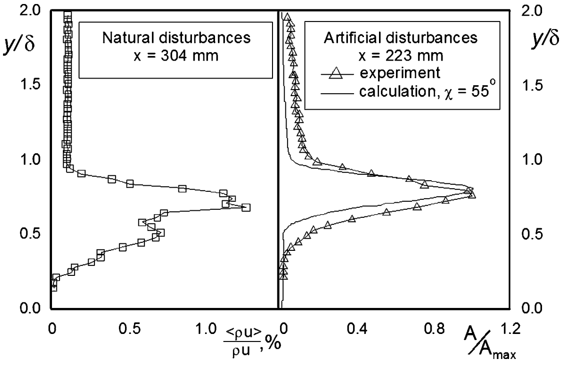

Fig. 7 Vertical distribution of integral pulsation amplitude.

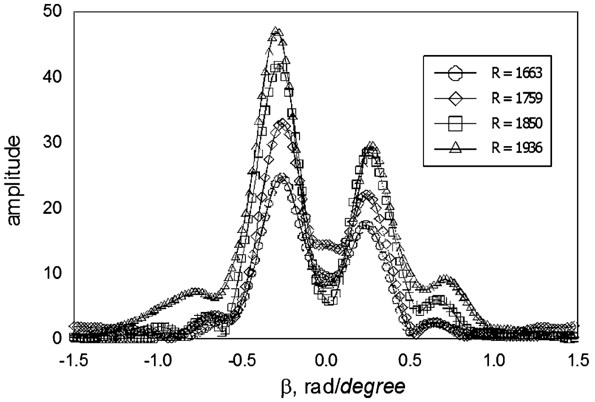

Fig. 8 β-spectra of the first mode artificial disturbances.

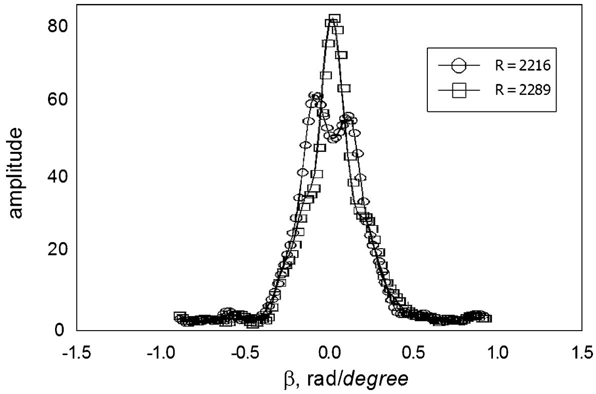

Fig. 9 β-spectra of the second mode artificial disturbances.

Conclusions

The present measurements confirm the presence of the second-mode disturbances in boundary layers on cones. Moreover, the spatial characteristics of the disturbances and growth rates of the waves, of both the first and second instability modes, are obtained and agree well with available experimental data and with linear stability theory predictions for compressible boundary layers.

The rapid growth of the amplification rates of pulsations corresponding to the second mode is observed downstream of the location where the boundary layer absorbs the entropy layer. The same behavior was also observed by Stetson et al.[4] To explain this result, Stetson et al. put forth a hypothesis that, at this location, forced amplification of disturbances takes place. This hypothesis is based on the fact that it is observed in the experiments of Stetson et al. that there is a high level of flow pulsations in the entropy layer comparable with the pulsation level in the boundary layer or even exceeding it. According to this hypothesis, these external pulsations can act as forcing disturbances impinging onto the boundary layer at the point where the boundary layer absorbs the entropy layer and promoting the growth of boundary-layer disturbances. Although our experiments reveal a weak intensity of flow pulsations in the entropy layer, the boundary-layer disturbances do display a rapid growth. Thus, the behavior of the boundary-layer disturbances is similar to that observed in Ref. 4, but the pulsations in the entropy layer are too small to have an effect on the boundary layer. This casts doubt on the hypothesis advanced in Ref. 4, in view of the fact that Mack's theory implies no influence of external disturbances on the growth rates.

Acknowledgment

The work was supported by the Russian Foundation for Basic Research (Grant 05-01-00349).

References

[1] Mack, L. M., "Boundary Layer Stability Theory," Jet Propulsion Lab., Document 900-277, Rev. A, Pasadena, CA, May 1969.

[2] Stetson, K., Thompson, E., Donaldson, J., and Siler, L., "A Comparison of Planar and Conical Boundary Layer Stability and Transition at a Mach Number of 8," AIAA Paper 91-1639, July 1991.

[3] Wilkinson, S., "A Review of Hypersonic Boundary Layer Stability Experiments in a Quiet Mach 6 Wind Tunnel," AIAA Paper 97-1819, June–July 1997.

[4] Stetson, K., Thompson, E., Donaldson, J., and Siler, L., "Laminar Boundary Layer Stability Experiments on a Cone at Mach 8, Part 2: Blunt Cone," AIAA Paper 84-006, July 1984.

[5] Schneider, S. P., "Hypersonic Laminar Instability on Round Cones near Zero Angle of Attack," AIAA Paper 2001-0206, Jan. 2001.

[6] Arnal, D., Maslov, A. A., Sidorenko, A. A., and Shiplyuk, A. N., "Leading Edge Receptivity of Hypersonic Boundary Layer on a Flat Plate," *Journal of Fluid Mechanics*, Vol. 426, 2001, pp. 73–94.

[7] Whitfield, J. D., and Dougherty, N. S., Jr., "A Survey of Transition Research at AEDC," Paper 25, AGARD Conf. Proceedings "Laminar–Turbulent Transition," AGARD Symposium, Copenhagen, May 1977.

[8] Maslov, A. A., Kosinov, A. D., and Shevelkov, S. G., "Experiments on the Stability of Supersonic Laminar Boundary Layers," *Journal of Fluid Mechanics*, Vol. 219, 1990, pp. 621–633.

[9] Malik, M. R., "Prediction and Control of Transition in Supersonic and Hypersonic Boundary Layers," *AIAA Journal*, Vol. 27, No. 11, 1989, pp. 1487–1493.

[10] Rotta, N. R., "Effects of Nose Bluntness on the Boundary Layer Characteristics of Conical Bodies at Hypersonic Speeds," New York Univ. Rept., NYU-AA-66-66, Nov. 1966.

[11] Stetson, K., Thompson, E., Donaldson, J., and Siler, L., "Laminar Boundary Layer Stability Experiments on a Cone at Mach 8, Part 1: Sharp Cone," AIAA Paper 83-1761, July 1983.

[12] Gaponov, S. A., and Maslov, A. A., *Disturbance Development in Compressible Flows*, Nauka, Novosibirsk, Russia, 1980, p. 144 (in Russian).

[13] Poggie, J., and Kimmel, R. L., "Disturbance Evolution and Breakdown to Turbulence in a Hypersonic Boundary Layer: Instantaneous Structure," AIAA Paper 97-0556, Jan. 1997.

T. Lin
Associate Editor